2019 Rock Dynamics Summit– Aydan et al. (eds)
© 2019 Taylor & Francis Group, London, ISBN 978-0-367-34783-3

# Effects of fault geometry and subsurface structure model on the strong motion and surface rupture induced by the 2014 Kamishiro Fault Nagano Earthquake

N. Iwata & R. Kiyota
*Chuden Engineering Consultants Co., Ltd., Hiroshima, Japan*

Ö. Aydan
*Department of Civil Engineering, University of the Ryukyus, Okinawa, Japan*

T. Ito
*Institute of Fluid Science, Tohoku University, Sendai, Japan*

F. Miura
*Graduate School of Science and Engineering, Yamaguchi University, Yamaguchi, Japan*

ABSTRACT: The authors used a three-dimensional finite element method (3D-FEM) to examine a series of fault rupture simulations for the 2014 Northern Nagano Earthquake and simultaneously estimate the displacement and strong motions. The computational results confirmed that the maximum responses of ground motions and displacement could be simultaneously evaluated using the appropriate constitutive parameters and fine FEM mesh. However, the duration of the acceleration response and shape of the surface displacement waves were not well simulated. In this study, we examined the influence of the fault bend at a shallow depth and P- and S-wave velocity structure models based on a geological survey. As a result, by taking account of bending of the fault plane and the elastic velocity structure at a shallow depth, it was possible to perform a seismic behaviour analysis using the 3D-FEM approach.

## 1 INTRODUCTION

Fault rupture simulations have been performed mainly for the reproduction and prediction of strong motions. After the 1999 Chi-Chi and Kocaeli earthquakes damaged many important structures as a result of surface rupture, the displacement and inclination of the ground surface caused by fault rupture have become significant issues in engineering. Many prediction methods for strong motion, displacement and inclination of the surface ground have been suggested. However, most analytical methods do not evaluate displacement and strong motions at the same time. Furthermore, the parameters adopted in these methods (fault length, slip on fault, stress drop, etc.) are empirically determined and the dynamic destruction process is not taken into account. Therefore, it is difficult to evaluate strong motions of magnitude nine, the seismic response around the epicentre and surface rupture with few observed data.

The authors have examined a series of fault rupture simulations to simultaneously estimate the displacement and strong motions at the ground surface using a three-dimensional finite element method (3D-FEM) considering the dynamic destruction process of the fault plane. This analytical method and modelling of faults was proposed by Toki & Sawada (1988) and Mizumoto et al. (2005). The fault plane was assumed to be discontinuities of bedrock and was modelled by joint elements, and shear failure occurred at the hypocentre and spread to the surrounding areas with increasing shear stress. Iwata et al. (2018) conducted a fault rupture simulation for the 2014 Northern Nagano Earthquake, which was induced by the Kamishiro Fault ($M_w$ 6.3). The computational results confirmed that the maximum responses of the ground motion and displacement could be evaluated using the appropriate constitutive parameters and a fine FEM mesh with a size less than 150 m. However, the duration of the acceleration response and shape of the surface displacement response were not well simulated, partly because the fault plane was assumed to be a straight planar feature and the bedrock was assumed to be homogeneous.

In this study, we examined the influence of a fault bend at a shallow depth and the S-wave velocity structure model based on a geological survey. In addition, we examined the influence of the initial stress distribution on the fault plane.

## 2 OUTLINE OF ANALYTICAL METHOD

If the equation of motion involves the rupture movement of the fault plane, it is necessary to treat the motion as a nonlinear problem. Therefore, it is appropriate to obtain a solution for the equation of motion, not in the frequency domain but rather in the time domain. The destruction process of dislocation and the dynamic behaviour of the ground are calculated by solving the equation of motion using the stress drop of the dislocation as the external force. The equation of motion at time step $n$ is written as

$$[M]\{\ddot{u}\}_n + [C]\{\dot{u}\}_n + [K]\{u\}_n = \{F(n,s)\} \quad 1$$

where $[M]$, $[C]$ and $[K]$ are mass, damping and stiffness matrix, respectively. $\{\ddot{u}\}$, $\{\dot{u}\}$, $\{u\}$ are acceleration, velocity and displacement vector, respectively. $\{F(n,s)\}$ is the external force vector calculated from the dynamic stress drop where $n$ and $s$, respectively, stand for the time step and nodal pairs where the fault rupture takes place. The damping matrix $[C]$ is obtained from the linear combination of $[M]$ and $[K]$, which is called Rayleigh damping. Equation (1) is solved using Newmark's $\beta$ method, with $\beta = 0.25$, $\gamma = 0.5$ at each time interval. To solve the nonlinear equation of motion, we employed the load transfer method using the initial stiffness method (Toki & Sawada, 1988, Tsuboi & Miura, 1996).

The fault plane was modelled by joint elements shown in Figure 1. The shear springs $K_s$, $K_r$ and normal spring $K_n$ are connected between nodal points of the solid elements, and sliding occurs according to the Mohr–Coulomb failure criterion. When the calculated shear stress $\tau$ is less than the peak stress $\tau_y$, the stress–deformation relationship is linear with the joint stiffness $K_s$, $K_r$. Sliding takes place if the shear stress $\tau$ reaches the peak stress $\tau_y$, and a stress drop occurs. The shear stress becomes equivalent to the residual strength $\tau_r$, and the stress drop $\Delta\tau_d$ ($= \tau_y - \tau_r$) is released and spreads to nearby elements. In this way, the released stress drop at the hypocentre is triggered and shear failure spreads to the surrounding areas with increasing shear stress.

## 3 OVERVIEW OF THE 2014 NORTHERN NAGANO EARTHQUAKE

The 2014 Northern Nagano Earthquake had a moment magnitude of 6.3. It occurred at 22:08 JST on November 22nd, in the northern part of Nagano

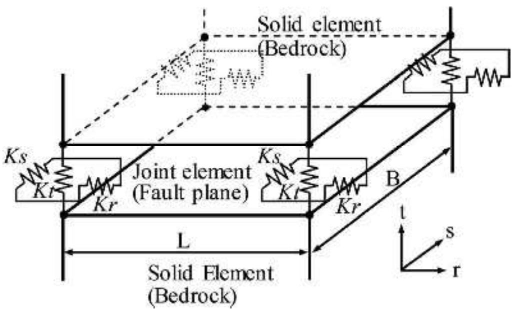


Figure 1. Schematic diagram of joint element.

Prefecture. The slip sense was estimated as thrust faulting with a left–lateral strike slip. There have been many reports by various organizations about the fault geometry and seismic moment. According to the F-net centroid moment tensor solution catalogue (F-net 2014) of the National Research Institute for Earth Science and Disaster Prevention (NIED), the seismic moment $M_0$ was $2.76 \times 10^{18}$ N·m, the fault plane was dipping downwards at N16E–50E, the rake angle was 65° and the focal depth was estimated at 5 km. On the other hand, the aftershock activity indicated a non-planar, bending fault plane, which consisted of two planar faults: the shallow plane with a dip angle of 40° connected to a deep plane with a dip angle of 60° at 4 km depth (Panayotopoulos, 2016).

Figure 2 shows the acceleration records at K-NET Hakuba station, which is one of the strong motion stations of the dense strong motion network operated by the NIED. It is located approximately 0.5 km from the surface rupture in the west, on the footwall side of the earthquake fault. The maximum accelerations are 570 Gal horizontally and 278 Gal vertically. The displacement response was calculated using the EPS method proposed by Aydan & Ohta (2011), which is an integration technique for obtaining ground motions in consideration of device operation features, fault rupture duration and arrival time difference of the P- and S-waves. From these results, the residual displacement was obtained as 24 cm horizontally and 10 cm vertically at the Hakuba site.

## 4 ANALYTICAL CONDITIONS AND PARAMETERS

### 4.1 *Analytical conditions*

To investigate the influence of the initial stress distribution in a fault plane, dip angle and velocity structure of the bedrock, we performed a series of fault rupture simulations under various conditions. The validity of the parameters and modelling was evaluated by comparison with the observed surface ground motions recorded at K-NET Hakuba station.

In previous studies, we assumed that the initial shear stress distribution shape was mountain type, in which the hypocentre is highest and the shear stress decreases towards the fault ends and becomes zero, as shown in Figure 3. However, the asperity type, in which the shear stress is concentrated only in protrusions on the fault plane, is used for predicting strong motions. Therefore, we compared the seismic response of asperity type with that of mountain type.

As for the dip angle, according to the aftershock activities and the results of seismic waveform inversion analyses (F-net 2014, JMA 2014 and Panayotopoulos, 2016), we compared the seismic response of the planar model with a dip angle of 50° or 60° and the bending model; the shallow plane with a dip angle of 40° connected the deep plane with a dip angle of 60° at 4 km depth.

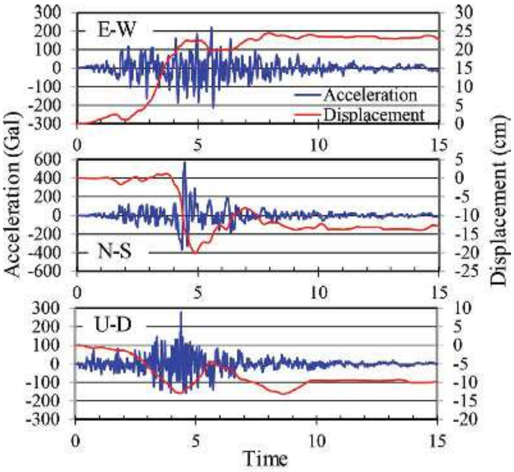


Figure 2. Acceleration records at K-NET Hakuba station and displacement time histories calculated by the EPS method.

As for the velocity of bedrock, in the previous studies we assumed that the bedrock was homogeneous and distributed uniformly with the ground surface. However, the elastic wave speed decreased as it neared ground surface at shallow depths. We examined parametric studies using horizontally layered model by the Japan Seismic Hazard Information Station (J-SHIS 2018): S-wave velocity was 1.1 km/s from the ground surface to 0.7 km in depth, 2.1 km/s at 0.7–2.6 km, 2.7 km/s at 2.6–2.7 km, 3.1 km/s at 2.7–3.0 km, 3.3 km/s at 3.0–8.0 km and 3.5 km/s below 8.0 km.

Other parameters were set as follows: the shear stiffness of a joint element was $1.0 \times 10^6$ kN/m$^3$, the normal stiffness was $3.0 \times 10^6$ kN/m$^3$ and the damping ratio was 0.03.

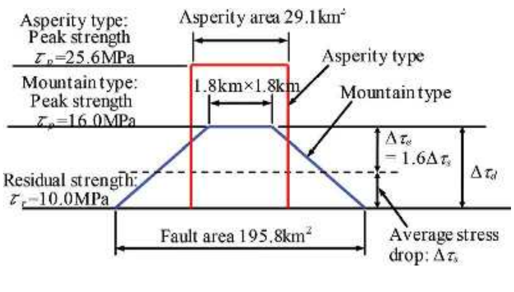


Figure 3. Schematic diagram of initial stress distribution.

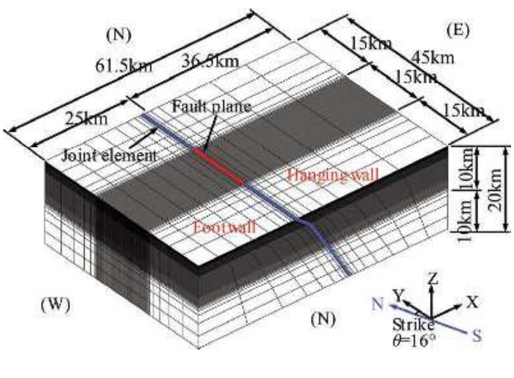


Figure 4. 3D FEM mesh.

## 4.2 *FEM model*

Figure 4 shows the FEM model with a bending fault plane. Joint elements were set up from the northern lateral boundary to the southern one, and the strength of joint elements located out of the fault plane was set to have a high value. The distance from the fault edge to the boundaries was more than the fault length (15 km), and viscous dampers were introduced at the lateral and bottom boundaries to absorb scattering wave energy.

## 4.3 *Stress on fault plane*

The average static stress drop $\Delta\tau_s$ in the fault plane was 2.3 MPa, calculated from the seismic moment and fault area according to the Recipe for Predicting Strong Ground Motions (Irikura 2006). In the mountain type stress distribution, the peak strength $\tau_y$ was determined based on the knowledge that the excess strength $\Delta\tau_e$ is 1.6 times the static stress drop $\Delta\tau_s$ (Andrew, 1976) and $\Delta\tau_d$ was made 6.0 MPa, as shown in Figure 3. In that figure, the shape of the peak stress distribution is a square, and the area of peak strength is calculated so that the volume of the truncated square pyramid described by a solid blue line equals that of the cube described by a dashed line. In the asperity type distribution, the area of asperity was calculated according to the 'Recipe', and $\Delta\tau_d$ was made 15.6 MPa by multiplying $\Delta\tau_s$ by the ratio of the fault area to the asperity area. The residual strength $\tau_r$ made 10.0 MPa sufficiently larger than the dynamic stress drop $\Delta\tau_d$. The shear stress at the hypocentre was assumed to be slightly larger than the peak strength $\tau_y$. The rake angle was 60° according to the results of the seismic waveform inversion analysis by the Japan Meteorological Agency (JMA 2014). The behaviour of thrust faulting with a left–lateral strike slip was reproduced by setting the initial shear stress in the rake angle.

# 5 ANALYSIS RESULTS

## 5.1 *Influence of initial stress distribution*

We carried out fault rupture simulations using various initial stress distributions: mountain type and asperity type, and compared the seismic moments and seismic response at the ground surface corresponding to that at K-NET Hakuba station. The parameters except the initial stress distribution were the same, the dip angle of fault plane was 50° and the bedrock was homogeneous.

Figure 5 shows the slip distribution in the fault plane in mountain-type case. The slip spreads from the hypocentre at the rake angle and reaches the ground surface. The maximum slip amount is 1.69 m, and the seismic moment is estimated as 5.93 × $10^{18}$ N·m, which is 2.1 times that of the observed value (M = 2.76 × $10^{18}$ N·m). Although the shape of asperity-type slip distribution is similar to that of mountain type, the maximum slip amount is 3.46 m and the seismic moment is estimated as 9.32 × $10^{18}$ N·m, which is 1.6 times that of mountain type.

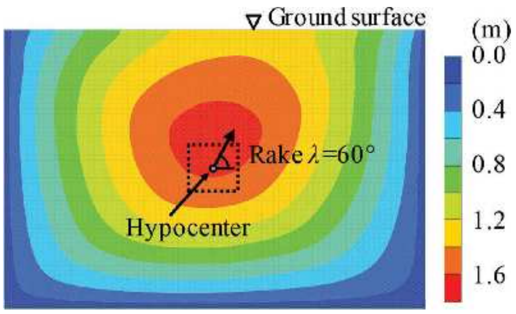


Figure 5. Slip distribution on the fault plane of Mountain type.

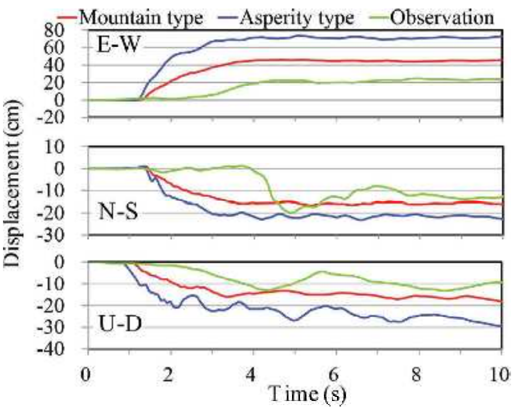


Figure 6. Comparison of analysed displacement waves using different initial stress distributions.

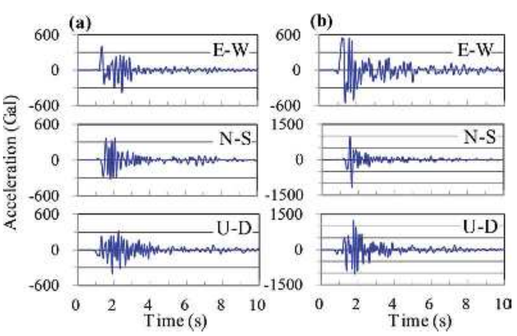


Figure 7. Comparison of acceleration waves using various initial stress distribution: (a) mountain type, (b) asperity type.

Figure 6 compares the analysed displacement waves at a distance of 0.5 km from the surface rupture with the observed records. The analysed residual displacements of mountain type are 1.3–2.0 times the observations, and those of asperity type are 1.5–3.5 times the observations.

Figure 7 shows a comparison of the analysed acceleration waves. The amount of stress drop for asperity type is so large that the destruction spreads over a stretch of area. Then, the maximum acceleration and residual displacement of asperity type become larger than those of mountain type and the duration of main shock becomes shorter. The maximum acceleration of asperity type is 1.4 times that of mountain type in the E–W direction and about 3.0 times in the N–S and U–D directions. Comparing the maximum accelerations, those of the mountain type are 1.9 times those of the observations in the E–W direction, 0.7 times in N–S direction and 1.5 times in U–D direction. The directivity effect of the fault rupture could not be reproduced in the acceleration response. It was necessary to conduct parametric studies of the rake angles. When the mesh size becomes less than 100 m, accelerations in the U–D direction become smaller. The vertical response could be improved using a finer FEM mesh.

From these results, even if the amount of stress drop in a fault plane was the same, the seismic response varied greatly according to the difference in initial stress distribution. When a stress drop based on the Recipe is adopted for a fault rupture simulation using the 3D-FEM, in some cases the analysed seismic response becomes considerably larger than expected.

## 5.2 *Influence of dip angle*

We performed fault rupture simulations using various dipping fault planes: a planar model with a dip angle of 50° or 60° and a bending model, and we examined the influence of the dip angle and shape of the fault plane. All parameters except the geometry of the fault plane were the same, the initial stress distribution was mountain type and the bedrock was homogeneous.

The slip distribution shape of the planar model with a dip angle of 60° was similar to that of the model with a dip angle of 50°. The maximum slip amount became 1.71 m, and the seismic moment was estimated as 5.93 × 10 N·m, which became slightly larger than the moment at 50°. Figure 8 shows the slip distribution with a bending fault plane. The slip distribution becomes discontinuous at a depth of around 4 km owing to the changing dip angle at that depth. The maximum slip on the shallow fault plane (dip angle of 40°) is 1.17 m and is larger around the hypocentre. The slide amount of the bending model is smaller than that of the planar model. The seismic moment was estimated as 4.45 × 10 N·m, which is 0.75 times that of the planar model with a dip angle of 50°.

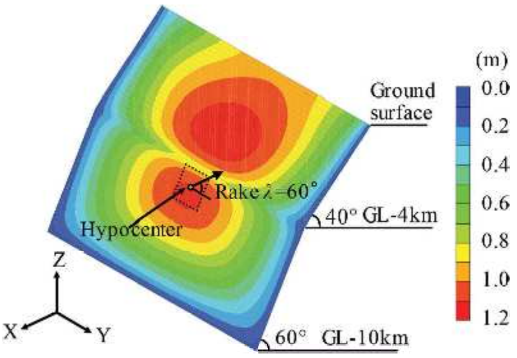


Figure 8. Slip distribution on the bending fault plane.

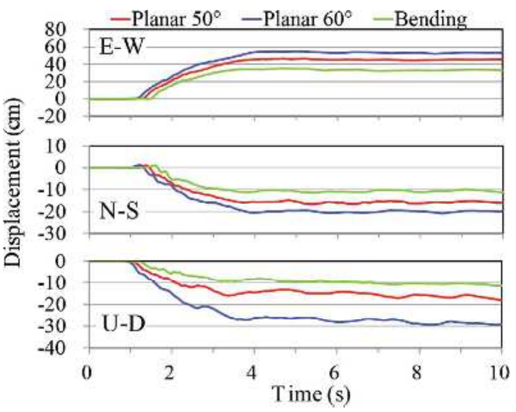


Figure 9. Comparison of analysed displacement waves using different fault geometry.

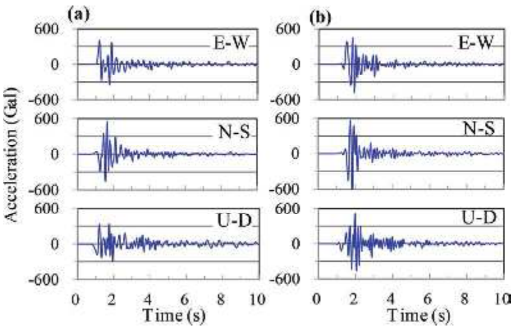


Figure 10. Comparison of acceleration waves using different fault geometry: (a) Planar 60°, (b) Bending 40+60°.

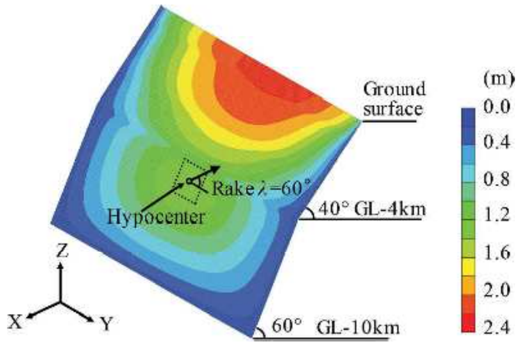


Figure 11. Slip distribution of horizontally layered model.

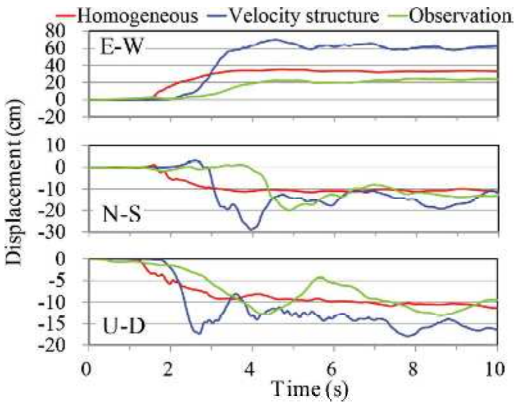


Figure 12. Comparison of analysed displacement waves using different velocity structures.

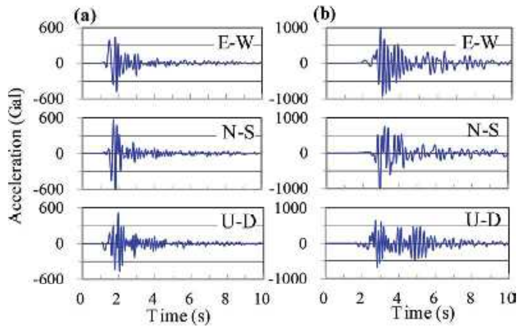


Figure 13. Comparison of acceleration waves using different velocity structures: (a) Homogeneous, (b) Horizontally layer.

Figure 9 compares the analysed displacement waves. The residual displacement of the 60° planar model is about 1.2 times that of the 50° planar model horizontally and 1.6 times vertically. The residual displacement of the bending model is about 0.7 times that of the 50° planar model.

Figure 10 shows the analysed acceleration waves. The waveform of the 60° planar model is similar to that of the 50° one shown in Figure 7(a). However, in the case of the bending fault, the peak acceleration becomes larger than that of the planar mode, the peak is delayed and the duration is extended. The maximum acceleration of the 60° planar model is at the same level as that of the 50° one in the E–W and U–D directions, and 1.5 times in N–S direction. The acceleration of the bending model is 1.2 times that of the 50° planar model in the E–W and U–D directions, and 2.0 times in N–S direction.

### 5.3 *Influence of velocity structure of bedrock*

To compare the influence of the velocity structure of bedrock, we conducted fault rupture simulations using homogeneous and horizontally layered models of the elastic wave velocity. In both cases, the initial stress distribution was mountain type and the fault shape was that of the bending model.

Figure 11 shows the slip distribution on the fault plane in the case of the horizontally layered model. The slip distribution becomes discontinuous at 4-km depth, like the homogeneous model shown in Figure 8. The maximum slip amount around the hypocentre is 1.34 m. The slippage become larger towards the ground surface, and the maximum slip amount is 2.36 m. The slippage of the horizontally layered model is larger than that of the homogeneous model. However, the seismic moment of the horizontally layered model (3.49 × 10 N·m) is smaller than that of the homogeneous model because the elastic wave velocity and stiffness of the surface layer are small.

Figures 12 and 13 show a comparison of the analysed displacement and acceleration waves at distances of 0.5 km from the surface rupture, respectively. When an elastic wave velocity structure is adopted, the time at which residual displacement begins to occur and the time of peak acceleration are delayed. The duration of the acceleration wave is extended, resulting in fluctuations. These behaviours resemble the observed records. However, the residual displacement and maximum acceleration become considerably larger.

Figure 14 shows the vertical displacement distribution at the ground surface in the E–W direction (orthogonal to the surface rupture). The gap in the surface rupture is 0.55 m in the homogeneous model and 1.3 m in the horizontally layered model. The distribution shape of the east side of the fault in the homogeneous model is approximately level at less than 1 km from the surface rupture and inclines gently at the outside. On the other hand, the vertical displacement of the east side of the fault in the horizontally layered model decreases sharply as it leaves the surface rupture. The inclination angle of the ground surface in the horizontally layered model

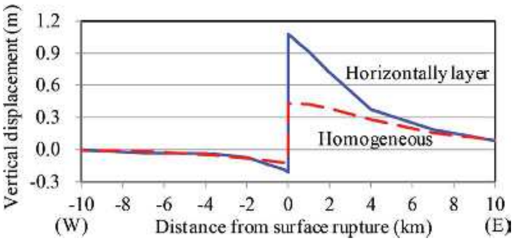


Figure 14. Comparison of vertical displacement distribution at the surface ground in E–W direction using various velocity structures.

is steeper than that in the homogeneous model. According to an InSAR analysis by the Geospatial Information Authority of Japan (GSI 2014), the incline of the ground surface on the east side of the surface rupture is steeper than that on the west side and the deformation occurs on the side of the surface rupture. Consequently, when an elastic wave velocity structure is adopted, the analysis result can be brought closer to the actual deformation.

## 6 CONCLUSIONS

In this study, we performed a series of fault rupture simulations using the 3D-FEM for the 2014 Northern Nagano Earthquake and evaluated the influences of the initial stress distribution on the fault plane, dip angle and velocity structure of the bedrock. The findings obtained from this study can be summarized as follows:When the amount of stress drop was defined based on the Recipe, the seismic moment, acceleration response and residual displacement were larger than the observed records.The analysed seismic response using the initial stress distribution of asperity type was larger than that of mountain type because the stress drop was larger and more rapidly released.The slip in the fault plane and displacement response of the bending fault model were smaller than those of the planar model. However, the acceleration response was larger.As the elastic velocity of the surface layer decreases, the seismic response and slippage became larger. However, the seismic moment became smaller because the stiffness of the surface layer was small.

By taking into account the bending of the fault plane and the elastic velocity structure at a shallow depth, it was possible to make the seismic behaviour analysed by the 3D-FEM approach the observation. However, the maximum acceleration and residual displacement were greater than the observations. Therefore, it is necessary to examine a setting method for the parameters and a model to reproduce the actual values.

## REFERENCES

Andrews, D.J. 1976. Rupture velocity of plane strain shear racks, *J. of Geo. Res.*, Vol. 81, No. 32, 5679–5687.

Aydan, O. & Ohta, Y. 2011. The erratic pattern screening (EPS) method for estimation of co-seismic deformation of ground from acceleration records and its application, *Seventh National Conf. on Earth. Eng.*, Turkey.

F-net (Full Range Seismograph Network of Japan), National Research Institute for Earth Science and Disaster Resilience. 2014. Topics: The 2014 North Nagano Earthquake (in Japanese) http://www.hinet.bosai.go.jp/topics/n-nagano141122/?LANG=en.

GSI (Geospatial Information Authority of Japan). 2014. Crustal deformation associated to the Northern Nagano earthquake observed by the "Daichi-2" ALOS-2 satellite (in Japanese). http://www.gsi.go.jp/BOUSAI/h26-nagano-earthquake-index.html.

Irikura, K. 2006. Predicting strong ground motions with "Recipe", *Bull. Earthq. Res. Inst. Univ. Tokyo*, 81: 341–352.

Iwata, N., Kiyota, R., Adachi, K., Takahashi, Y., Aydan, Ö., Miura, F. & Ito, T. 2018. Simulation of strong motions and surface rupture of the 2014 Northern Nagano Earthquake. *Proc. of the 3rd inter. conf. on Rock dynamics and applications (ROCDYN-3), Norway*: 541–546.

JMA (Japan Meteorological Agency). 2014. News release document about the earthquake of North Nagano on November 22, 2014 about 22:08 (in Japanese).

J-SHIS (Japan Seismic Hazard Information Station). 2018. Subsurface structure.

Mizumoto, T., Tsuboi, T. & Miura, F. 2005. Foundamental study on failure rupture process and earthquake motions and near a fault by 3D-FEM. *Journal of Japan Society of Civil Engineers* 780/I-70: 27–40 (in Japanese with English abstract).

Panayotopoulos, Y., Hirata, N., Hashima, A., Iwasaki, T., Sakai, S. & Sato, H. 2016. Seismological evidence of an active footwall shortcut thrust in the Northern Itoigawa–Shizuoka Tectonic Line derived by the aftershock sequence of the 2014 M6.7 Northern Nagano earthquake. *Tectonophysics* 679: 15–28.

Toki, K. & Sawada, S. 1988. Simulation of the fault rupture process and near filed ground motion by the three-dimensional finite element method. *Proc. of 9th World Conf. on Earth. Eng., Japan*, Vol. II: 751–756.

Tsuboi, T. & Miura, F. 1996. Simulation of stick-slip shear failure of rock masses by a nonlinear finite element method. *Journal of Japan Society of Civil Engineers* 537/I-35: 61–76 (in Japanese with English abstract).